Original Research

The effects of low-frequency ultrasound and microbubbles on rabbit hepatic tumors

Zhi-Yong Shen[1], Gan-Lin Xia[1], Ming-Feng Wu[1], Min-Xin Shi[1], Fu-Lin Qiang[1], E Shen[2] and Bing Hu[2]

[1]Department of Radiology, Nantong University Affiliated Nantong Tumor Hospital, Nantong 226361, Jiangsu Province, China; [2]Department of Ultrasound in Medicine, Shanghai Institute of Ultrasound in Medicine, Shanghai Jiao Tong University Affiliated Sixth People's Hospital, Shanghai Jiao Tong University School of Medicine, Shanghai 200233, China
Corresponding authors: Bing Hu. Email: hub1523@126.com and Fu-Lin Qiang. Email: ntumoryz@163.com

Abstract

High-intensity focused ultrasound in combination with microbubbles (MBs) is able to inhibit the growth of VX2 rabbit liver tumors *in vivo* and prolong the survival time of the animals. In this study, we attempt to investigate the feasibility of VX2 tumor growth inhibition using low-frequency ultrasound (US)-mediated MB disruption. Forty-eight New Zealand rabbits with hepatic VX2 tumors were divided into four groups: control, MBs group, low-frequency US group, and US + MB group. The parameters of the US were 20 kHz, 2 W/cm^2, 40% duty cycle, 5 min, and once every other day for 2 weeks. At the end of the therapy experiment, 24 rabbits were euthanized, and the cancers were collected and cut into five sections for histological examination, immunohistochemistry, laser confocal microscopy, western blotting assays, and transmission electron microscopy (TEM). Another 24 rabbits were saved, and overall survival time was recorded. The tumor volumes in control, MB, US, and US + MB groups were 6.36 ± 0.58, 5.68 ± 0.42, 5.29 ± 0.26, and 2.04 ± 0.14 cm^3, respectively (US + MB versus the other three groups, $P < 0.01$). Tumor cells manifested coagulation necrosis with internal calcification. Hematoxylin and eosin (H–E) staining revealed interstitial hemorrhage and intravascular thrombosis. The intensity of cyclooxygenase-2 (COX-2), and vascular endothelial growth factor (VEGF) in the US + MB group in the immunohistochemical staining, laser confocal microscopy, and western blotting assays was lower than that of the other three groups ($P < 0.05$). TEM of the US + MB group revealed vascular endothelial cell wall rupture, widened endothelial cell gaps, interstitial erythrocyte leakage, and microvascular thrombosis, while intact vascular endothelial cells and normal erythrocytes in the tumor vessels were observed in control, MB, and US groups. Rabbits treated with US + MB had a significantly longer overall survival than those in the other three groups ($\chi 2 = 9.328$, $P = 0.0242$). VX2 tumor growth could be inhibited by cavitation induced using low-frequency US and MB.

Keywords: Ultrasound, low frequency, microbubble, cavitation, hepatic, VX2 tumor, rabbit

***Experimental Biology and Medicine* 2014; 239: 747–757. DOI: 10.1177/1535370214525320**

Introduction

Microbubbles (MBs) are small gas-filled microspheres that have specific acoustic properties that originally make them useful as a contrast agent in ultrasound (US) imaging.[1] When administered into a body cavity or the cardiovascular system, MBs are capable of increasing the intensity of backscattered US[2] and the improved sensitivity of US to microcirculation assists in characterization of scanned lesions and discrimination of malignant tumors from benign ones.[3] Nevertheless, in addition to contrast-enhancing ability, the trends in the developments in later generations of MBs agents have moved away from diagnostic efficacy and toward therapeutic modalities. Unlike rigid particles, MBs are highly compressible and are able to oscillate, i.e. repeatedly expand and contract in response to the pressure changes of an US pulse.[4] The MBs oscillate, grow, and collapse coherently under the influence of the varying pressure field of a sound wave in a fluid medium. This process can generally be defined as cavitation.[5,6] There are two distinct types of acoustic cavitation activity. Non-inertial (or stable) cavitation bubbles persist for a relatively large number of acoustic cycles, where the bubble radius varies about an equilibrium value that is determined by the operating frequency.[5] Under stable cavitation, the phenomenon of microstreaming is induced by the interaction of the US and MBs. Periodic radial oscillations of gas bubbles in blood lumen create complex steady-state streaming patterns within the lumen in the vicinity of the oscillating bubble surface.

This phenomenon is termed acoustic micro-streaming.[7,8] Micro-streaming is associated with stable cavitation. Inertial (or transient) cavitation bubbles grow faster, expanding two to three times their resonant size, where they oscillate unstably and finally collapse in a single compression half-cycle.[9] Upon collapse of cavitation bubbles, a strong flow field is generated that accounts for two effects: first, detachment of cells from the substrate and second, the temporary opening of cell membranes followed by molecular uptake, a process called sonoporation.[10,11] The interaction of cavitation bubbles with a boundary in fluid medium occurs frequently in a wide range of engineering and biomedical applications.[12,13] The violent collapse of the bubbles and subsequent shockwave emission or high-speed liquid jet formation have initially been reported to be associated with erosion damage on solid surfaces in hydraulic machinery.[12] However, the power of cavitation has also been harnessed in biomedical applications to improve the disintegration of kidney stones in shockwave lithotripsy,[14] to facilitate targeted drug and gene delivery,[15,16] and to enhance the efficacy of high-intensity focused ultrasound (HIFU) in cancer therapy.[17] It is usually accepted that the primary mechanism for structurally altering intact cells is inertial cavitation, where these alterations include both irreversible damage[18] as well as non-destructive increases in membrane permeability.[19] A variety of phenomena have been reported to occur when a cavitating bubble collapses in an open medium. The influence of transient cavitation will be more significant at lower ultrasonic frequencies.[20] The large and rapid reduction in volume experienced in a bubble undergoing inertial collapse can produce a significant rise in pressure and temperature (several thousand degrees centigrade or more).[13] It is also worth noting that at excitation frequencies much lower than those used in US imaging and at relatively high intensities, there is the potential for the formation of free radicals and toxic chemicals, such as hydrogen peroxide (H_2O_2), which may affect cells.[21] Our previous research results indicate that low-intensity US with MBs may have antiangiogenic effects on subcutaneous tumors in nude mice.[22] Tumor growth in small animals such as rats can be inhibited by the cavitation induced by US and MBs.[23] HIFU combined with MBs can inhibit the growth of VX2 rabbit liver tumors *in vivo* and prolong the survival time of the animals.[24] However, HIFU requires sophisticated instruments (guided ultrasonographic imaging and therapeutic transducers), complex therapeutic plans, a long treatment time (ranging from 2 to 8 h[25]), and has several complications (fever and US-induced skin burns). In contrast, low-frequency US (20–100 kHz) has been demonstrated to be more potent in enhancing transdermal delivery and penetration compared with high-frequency US (more than 2 MHz).[26] Another benefit is that the cavitation effects of low-frequency US are more intense and the thermal effects are less significant than that at higher frequencies[20]; therefore, skin burns could be obviously alleviated. So far, *in vivo* carcinoma growth inhibition in VX2 rabbit liver tumors by low-frequency US (i.e. 20 kHz) has not been reported. The objective of the present study was to explore the effects of low-frequency US combined with MBs on the hepatic tumors of New Zealand rabbits.

Materials and methods

Animal protocol and tumor inoculation

The experiments were performed with New Zealand white rabbits that weighed 2.0–2.5 kg (average 2.2 kg). The experiments were approved by the Animal Care Committee of Nantong University Medical School, Jiangsu, China and were performed in accordance with the institutional guidelines. The animals were anesthetized with an intravenous injection of 30 mg/kg pentobarbital. VX2 carcinoma was used to establish the model of hepatic tumors. VX2 carcinoma is an anaplastic squamous cell carcinoma that is derived from a virus-induced papilloma in wild rabbits but appears as a carcinoma in the domestic species. VX2 tumors were first grown for 2 weeks on the hind legs of carrier rabbits and then were harvested after they reached a size of 1.5 cm. The harvested tumors were placed into saline solution and cut into cubes of 1 mm^3. Only portions of tumor tissue that did not display any macroscopic signs of necrosis were used. Abdomens of the recipient rabbits were shaved and prepared with povidone iodine, and a midline subxiphoid incision was made. The anterior surface of the liver was exposed, and one of the prepared cubes of tumor tissue was implanted in the left lobe of the liver using a forceps. The outlet of the inoculated area was blocked by cotton sponge rubber. This method allowed the growth of a solitary, well-demarcated tumor. There was only one inoculation site in each liver. Proper aseptic technique was rigorously observed during each inoculation. After surgery, the animals were returned to their cages, kept warm, and monitored in the animal laboratory until they recovered from anesthesia. An iU22 ultrasound system (Philips, Bothell, Washington, USA) with a 12–15 MHz broadband linear probe was used to monitor the tumor growth every day after tumor inoculation. VX2 carcinoma nodules reaching 0.8–0.9 cm in diameter were considered appropriate for low-frequency US treatment. The period for tumors to reach the size of 0.8 cm ranged from 12 to 13 days. All inoculations were performed by the same individual investigator, who inoculated specimens of the same tumor into all rabbits to minimize inter-animal variations in tumor growth rate.

Experimental protocol

Tumor therapy and experimental protocol. In the study, 48 tumor-bearing rabbits were randomly divided into four groups, with 12 rabbits in each group. The groups were the A group: negative control (sham treatment); B group, MBs; C group, low-frequency US; and D group, US + MB. The MBs used were an ultrasound contrast agent (SonoVue: Bracco SpA, Milan, Italy).[27] The rabbits were anesthetized by auricular vein injection using 30 mg/kg pentobarbital. It is a routine site for vein injection in a rabbit.

After successful anesthesia, an ultrasonic instrument-iU22 ultrasound system (Philips, Bothell, Washington, USA) was used for tumor location before insonication of liver tumors. The hepatic tumors were subsequently sonicated using focused low-frequency US transducer manufactured by Taizhou Research Institute of Ultrasound Technology in Jiansu province, China. The probe was

placed on the shaved abdominal skin of rabbits, with an US transmission gel (A lotus medical ultrasonic coupling agent, Yi Jie Guangzhou Pharmaceutical Technology Co., Ltd, China) being interposed to ensure US propagation. The diameter of the therapeutic US transducer was approximately 24 mm. Low-frequency US parameters were set to 20 kHz, 2 W/cm^2, duty cycle 40% (on 2 s, off 3 s), and a duration of 5 min once every other day for 2 weeks. The US contrast agent was administered simultaneously with US wave irradiation via the auricular vein of rabbits by continuous infusion (the flow rate was 0.2 mL/min). The dose of the contrast agent administered was 1 mL (0.4 mL/kg) per rabbit for each treatment. The concentration of the contrast agent was 1.8×10^9 MBs/mL. The tumor size of rabbits was obtained every 3 days using the US scanner (iU22 ultrasound system, Philips, Bothell, Washington, USA) (Figure 1). Tumors were measured every 3 days, and tumor volumes were calculated using the formula $V = 0.5\ ab^2$, where b and a are the shortest and longest diameters of the measured tumor, respectively.

Histologic examination

At the end of the therapy experiment, 24 rabbits with each group of six rabbits were euthanized, and the cancers were collected, cut into five sections for histology examination, immunohistochemistry, laser confocal microscopy, western blotting assays, and transmission electron microscopy (TEM). Tumor tissues for histology examination were fixed and embedded in paraffin, and each tumor was stained using H–E. Subsequently, the structure of the tumor cells was observed using light microscopy. A histopathologist blind to the study evaluated the findings using microscopy. Another 24 rabbits were saved, and the overall survival time was calculated.

Immunohistochemistry

Tumor samples for immunohistochemistry were fixed with formaldehyde, dehydrated with a graded alcohol series, and embedded in paraffin. The sections were incubated with primary antibodies against COX-2 and VEGF (Santa Cruz Biotechnology Inc., Santa Cruz, CA, USA) at a 1:100 dilution and subsequently incubated with the appropriate biotinylated secondary antibody as detailed previously.[28] Colorimetric detection was performed using a diaminobenzidine (DAB) detection kit (Boster Biological Technology Co. Ltd, Wuhan, China). Images were acquired using an Olympus BX51 microscope. The percentage of cells expressing the marker was classified qualitatively based on the intensity of the immunohistochemical staining and the percentage of cells that were stained as follows:[29] score 0,

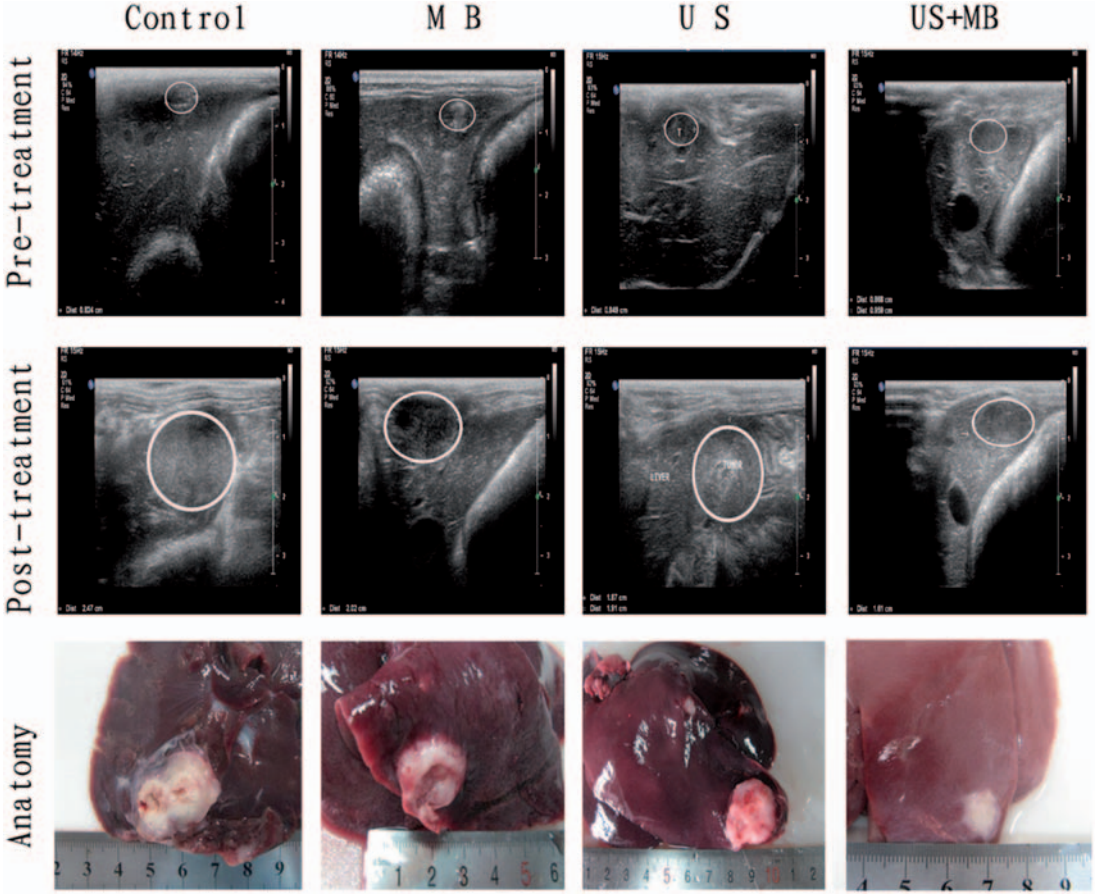

Figure 1 Representative ultrasound images prior to and following treatment and anatomies of tumors in the control, MB, US, and US + MB groups. (A color version of this figure is available in the online journal.)

intensity staining in 0–24% of cells; score 1, intensity staining in 25–49% of cells; score 2, staining in 50–74% of cells; and score 3, intensity staining in 75–100% of cells.

Confocal laser microscopy

Microassessment of vascular endothelium can be achieved in selected reasonable sized areas from tissue sections using laser confocal microscopy. Confocal microscopy constitutes a powerful state-of-the-art technique in the investigation of vessel structure and function in normal and pathological conditions, in relation to tumor treatment. In contrast to conventional wide-field fluorescent and light microscopy, images captured using confocal laser scanning microscopes displayed greatly improved clarity with successful elimination of out-of-focus background noise via the pinhole.[30] Confocal fluorescent microscopic studies of tumor tissue are possible using intrinsic green autofluorescent properties of tissue. The fluorescence expression and distribution pattern were observed using an Olympus FluoView FV500 confocal laser microscope. The digital image subtraction method was devised to eliminate autofluorescence. For each sample, green fluorescent protein expression and therapy efficiency were evaluated in six randomly chosen fields per section. After thorough washing in normal Tyrode's solution, samples were directly embedded in optimal cutting temperature compound and quickly frozen in liquid nitrogen for VEGF and COX-2 determination using confocal microscopy. Frozen 4 μm thick sections were spread over glass slides, allowed to dry for 1 h, and stored desiccated at −80°C until use. Tumor preparations were stained with either 12.5 μM fluo-3 acid or 10 μM sodium green acid for 15 min at room temperature. After several washes in Tyrode's buffer, the sections were mounted with a coverslip in 50% glycerol in phosphate-buffered saline (PBS). The excitation and emission wavelengths were 488 nm (10%) and >530 nm, respectively.

Western blotting assays

At the end of therapy experiment, some tumors of rabbits were collected followed by detection of protein expressions of COX-2 and VEGF by western blot assays. Tumor tissues were lysed in RIPA buffer (150 mM NaCl, 100 mM Tris–HCl, 1% Tween-20, 1% sodium deoxycholate, and 0.1% sodium dodecyl sulfate (SDS)) with 0.5 mM Ethylene Diamine Tetraacetic Acid (EDTA), 1 mM Phenylmethanesulfonyl fluoride (PMSF), 10 μg/mL aprotinin, and 1 μg/mL pepstatin. Proteins were subjected to SDS-polyacrylamide gelelectrophoresis (PAGE) and transferred to Polyvinylidene fluoride (PVDF) membranes, which were then treated with primary and secondary antibodies.

The membranes were incubated with primary antibodies against Cox-2 (1:1000; Santa Cruz Biotechnology) and VEGF (1:1000; Santa Cruz Biotechnology). Antibody binding was revealed by incubation with horseradish peroxidase-conjugated secondary antibodies (Santa Cruz Biotechnology) and an ECL Plus immunoblotting detection system (GE Healthcare Biosciences, Fairfield, CT, USA). Signals were quantified using NIH Image 1.63 software (National Institutes of Health, Bethesda, MD, USA).

TEM

Each tumor sample, ~1 mm^3, for TEM was fixed in 2% glutaraldehyde and PBS for 2 h at 4°C followed by PBS buffer and washed twice for 10 min. After treatment with 1% osmium tetroxide in PBS, specimens were fixed in 4°C for 2 h and dehydrated with 30%, followed by 50%, followed by 70% ethanol three times each for 10 min. The samples were then embedded in propylene oxide for 2 h and stained with lead citrate E. Finally, after sectioning, the specimens were examined using TEM (Philips CM-120; Philips, Eindhoven, The Netherlands).

Survival time follow-up

Survival time was calculated based on the date of tumor incubation and date of death. The survival time of the treated 24 rabbits with each group of six rabbits euthanized at the end of 15-day experiment was calculated using a right censoring survival model. The survival time of the remaining 24 rabbits with each group of six rabbits was followed up. The survival curves were calculated using the Kaplan–Meier method and were analyzed using the log-rank test.

Statistics

Statistical analysis was performed using SPSS version 11.0 (SPSS Inc.). The Student's *t*-test of tumor size was used to make a statistical comparison between groups. The immunohistochemistry, confocal microscopy, and western blot assays of the different treatment groups were analyzed statistically by applying a one-way Analysis of Variance (ANOVA) test. The survival curves were calculated using the Kaplan–Meier method and were analyzed using the log-rank test. All testing was performed using Prism 3.0 (GraphPad, San Diego, CA). Error bars were displayed as the standard error above the mean. Statistical significance was determined using $P < 0.05$.

Results

Effect of the combination of low US intensity and MBs on tumor growth

In the US + MB group, tumor coagulation necrosis and internal calcification (×200) were manifested. Diffused interstitial hemorrhage and vascular thrombus were also found at 2 weeks after treatment. The residual live neoplastic cells could be found only at the peripheral border area. In the control, MB, and US groups, intact live tumor tissues grew in a solid pattern without obvious vascular rupture and necrosis (Figure 2). The tumor growth curve of the control, MB, US, and US + MB groups are shown in Figure 3. On the 15th day after treatment, the tumor volume in the control, MB, US, and US + MB groups were 6.36 ± 0.58, 5.68 ± 0.42, 5.29 ± 0.26, and $2.04 \pm 0.14\,cm^3$, respectively. The tumor volume in the US + MB group was significantly smaller than those in the control, MB, and US groups (compared with the control group: $t = 15.18$, $P < 0.0001$; compared with MB group: $t = 10.79$, $P = 0.001$; compared with US group: $t = 9.12$, $P = 0.003$) (Figure 3).

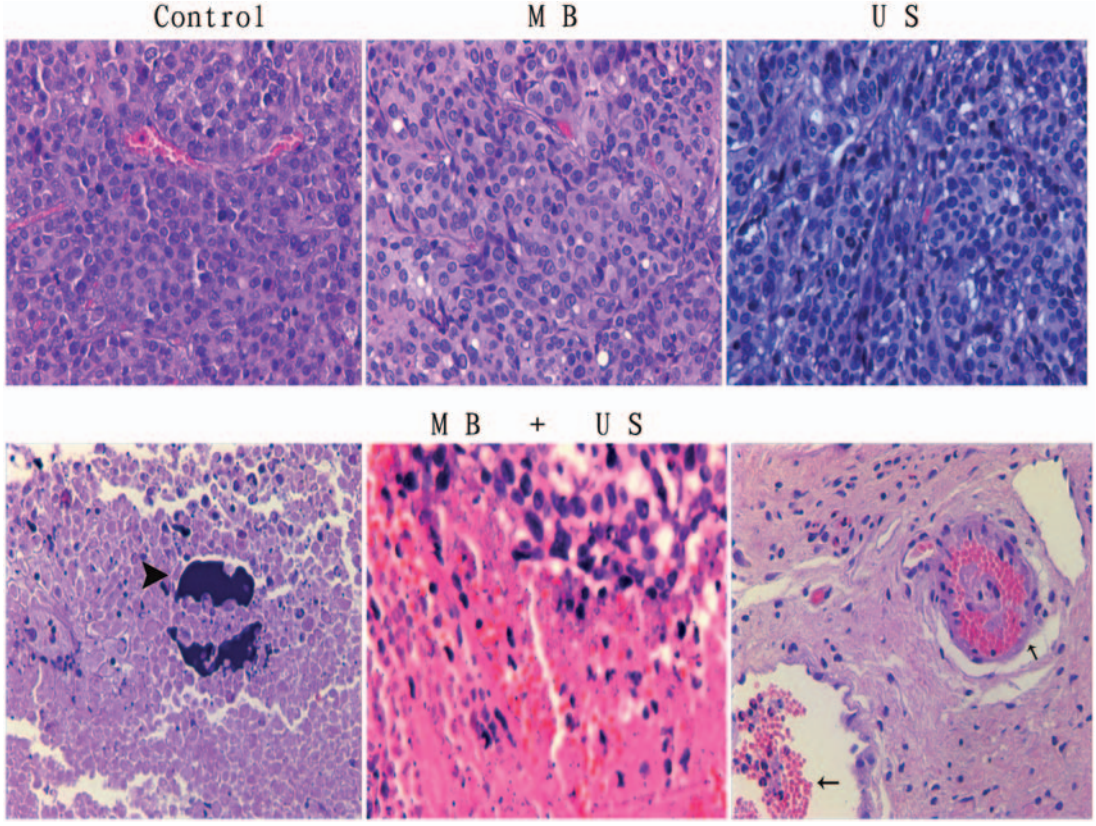

Figure 2 The H–E staining results for the control, MB, US, and US + MB groups (×200). Intact live tumor tissues in the control, MB, and US groups grew in solid pattern without obvious vascular rupture and necrosis. However, in the US + MB group, H–E staining revealed coagulation necrosis and calcification (arrow head), hemorrhage in tumor tissue and thrombogenesis (arrow) in the vessels. (A color version of this figure is available in the online journal.)

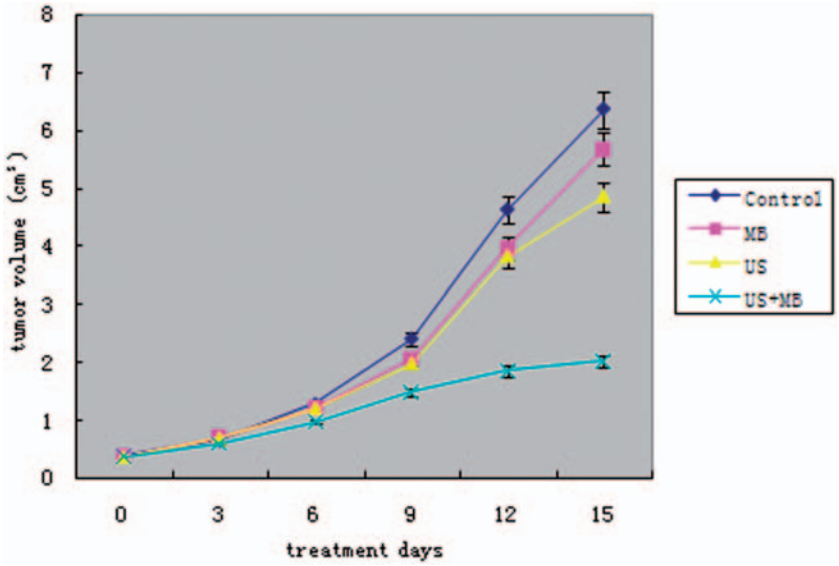

Figure 3 Tumor growth curve of the control, MB, US, and US + MB groups. The tumor volume was smaller in the US + MB group than in the control, MB, and US groups ($P < 0.01$). (A color version of this figure is available in the online journal.)

Effects of the combination of low US intensity and MBs on COX-2 and VEGF expression detected using immunohistochemistry, immunofluorescence, and western blot

Part one. According to immunohistochemistry, scores were classified as 0–3 based on the intensity of staining and the percentage of positive cells. The mean score of COX-2 in vascular endothelial cells and cytoplasm in the control, MB, US, and US + MB groups were 2.83 ± 0.19, 2.7 ± 0.32, 2.5 ± 0.16, and 1.33 ± 0.26, respectively. There were significant differences in protein expression among the four groups as determined using the ANOVA test, with $F = 17.23$ and $P = 0.0003$. In the MB and US group, the staining intensity decreased, but there was no significant difference compared with the control group ($P > 0.05$). However, in the US + MB group, the staining intensity of COX-2 was lower than in the other three groups ($P < 0.05$) (Figure 4). The mean score of VEGF in vascular endothelial cells and cytoplasm in the control, MB, US, and US + MB groups were 2.86 ± 0.12, 2.7 ± 0.21, 2.5 ± 0.18, and 1.43 ± 0.13, respectively. There were significant differences in protein expression among the four groups as determined using the ANOVA test, with $F = 16.36$ and $P = 0.0004$. In the MB and US group, the staining intensity decreased, but there were no significant difference compared with the control group ($P > 0.05$). However, in the US + MB group, the staining intensity of VEGF was lower than in the other three groups ($P < 0.05$) (Figure 4). Therefore, the combination of US and MB could lead to significant downregulation of the intensity of staining of COX-2 and VEGF protein (Figure 4).

The mean intensity values for VEGF in vascular endothelial cells and cytoplasm according to confocal laser microscopy in the control, MB, US, and US + MB groups were 82.74 ± 4.38, 76.65 ± 9.42, 68.51 ± 8.42, and 40.83 ± 5.68, respectively. There were significant differences in protein expression among the four groups as determined using the ANOVA test, with $F = 16.92$ and $P < 0.0001$. Using the Newman–Keuls multiple comparison test, a significant difference was found between the US + MB group and the other three groups ($P < 0.01$), but there was no significant difference between the control, MB, and US groups ($P > 0.05$) (Figure 5). The mean intensity values of COX-2 in the vascular endothelial cells and cytoplasm for the control, MB, US, and US + MB groups were 67.53 ± 7.77, 63.83 ± 8.94, 56.37 ± 9.79, and 28.21 ± 6.84, respectively.

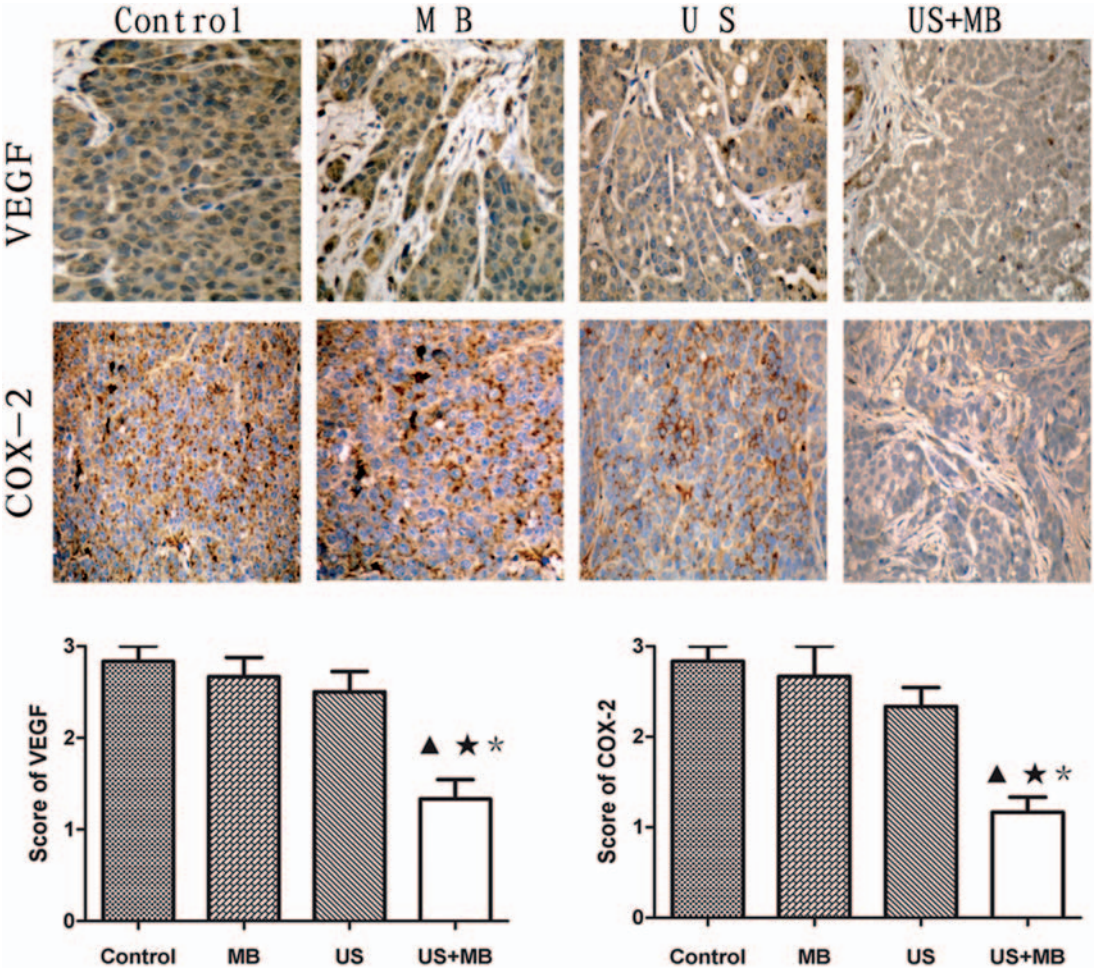

Figure 4 Immunohistochemistry results. In the US + MB group, the staining intensity of COX-2 and VEGF clearly decreased compared with the other three groups ($P < 0.05$). ▲$P < 0.05$ versus control group; ★$P < 0.05$ versus MB group; *$P < 0.05$ versus US group. (A color version of this figure is available in the online journal.)

There were significant differences in protein expression among the four groups as determined using the ANOVA test, with $F = 11.25$ and $P = 0.0002$. Using the Newman–Keuls multiple comparison test, a significant difference was found between the US + MB group and the other three groups ($P < 0.01$), but there was no significant difference between the control, MB, and US groups ($P > 0.05$) (Figure 5).

Part two. On western blot assays, the mean intensity ratio of VEGF to glyceraldehyde-3-phosphate dehydrogenase (GAPDH) in vascular endothelial cells and cytoplasm in the control, MB, US, and US + MB groups were 88.93 ± 4.33, 75.36 ± 11.56, 59.83 ± 6.56, and $40.33 \pm 3.56\%$, respectively. There were significant differences in protein expression among the four groups as determined using the ANOVA test, with $F = 21.26$ and $P < 0.0001$. Using the Newman–Keuls multiple comparison test, a significant difference was found between the US + MB group and other three groups ($P < 0.01$), but there was no significant difference between the control, MB, and US groups ($P > 0.05$) (Figure 6). The mean intensity ratio of COX-2 to GAPDH in the vascular endothelial cells and cytoplasm in the control, MB, US, and US + MB groups were 79.53 ± 4.93, 73.16 ± 6.92, 62.23 ± 5.82, and $31.33 \pm 6.21\%$, respectively. There were significant differences in protein expression among the four groups as determined using the ANOVA test, with $F = 23.21$ and $P < 0.0001$. Using the Newman–Keuls multiple comparison test, a significant difference was found between the US + MB group and the other three groups ($P < 0.01$), but there was no significant difference between the control, MB, and US groups ($P > 0.05$). Therefore, the protein expression of VEGF and COX-2 in the US + MB group was significantly lower than that in the control, MB, and US groups (Figure 6).

TEM results

TEM revealed vascular endothelial cell wall rupture, widened endothelial cell gaps, interstitial erythrocyte leakage, and vascular lumen thrombosis in the US + MB group. Most tumor cells appeared normal in the other three groups. Intact vascular lumen and normal erythrocytes in the tumor vessels were found in the control, MB, and US groups (Figure 7).

Survival time follow-up

Rabbits treated with US + MB had a significantly longer overall survival than those in the control, MB, and US groups ($\chi 2 = 9.328$, $P = 0.0242$) (Figure 8).

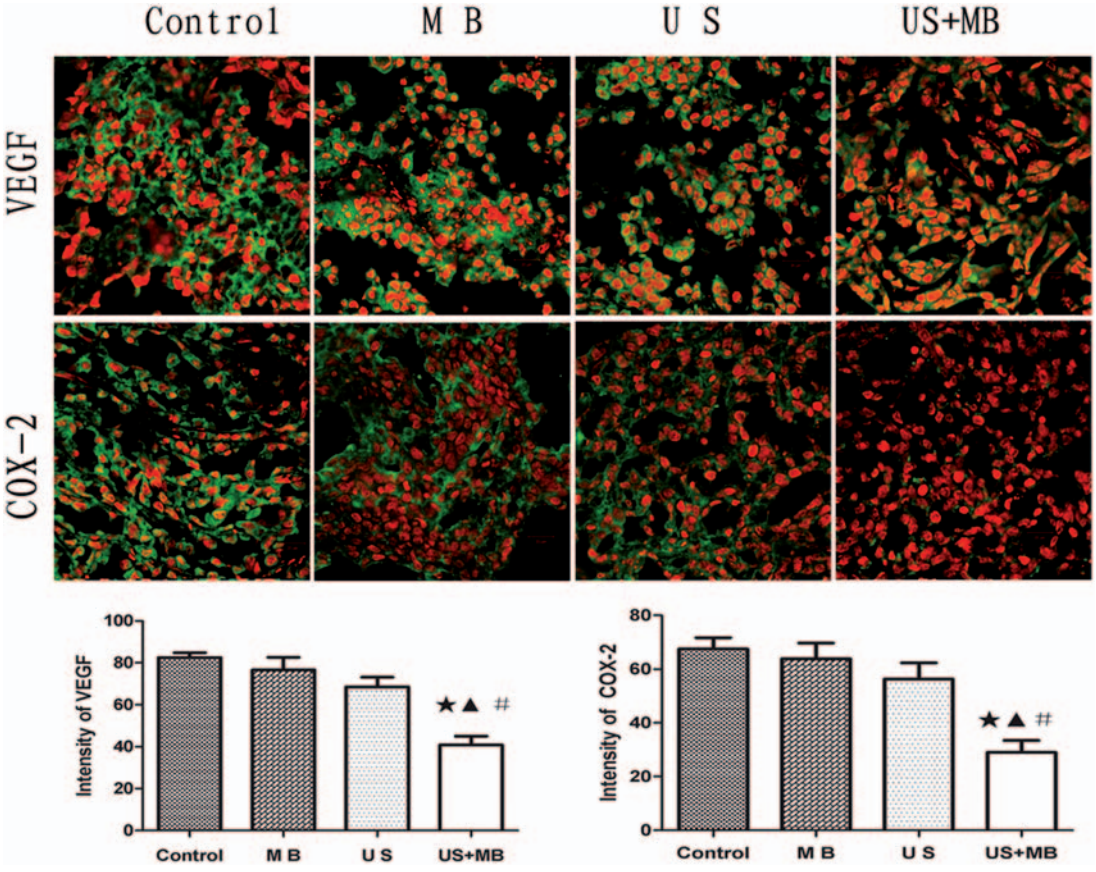

Figure 5 VEGF and COX-2 protein intensity of each group by confocal laser scanning microscopy (CLSM). There was a significant difference in VEGF between the US + MB group and the other three groups (★ $P < 0.01$ versus control group; ▲ $P < 0.01$ versus MB group; #$P < 0.01$ versus US group). There was a significant difference of COX-2 level between the US + MB group and the other three groups (★ $P < 0.01$ versus control group; ▲ $P < 0.01$ versus MB group; #$P < 0.01$ versus US group). (A color version of this figure is available in the online journal.)

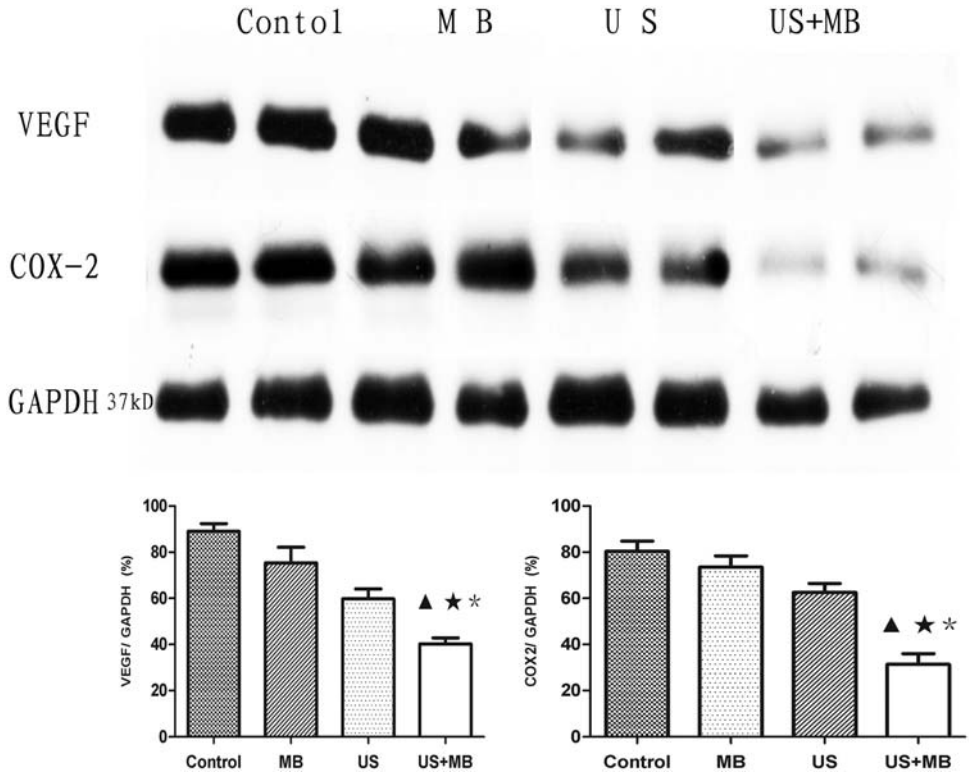

Figure 6 COX-2 and VEGF protein intensity ratio of each group by western blotting. There was a significant difference in COX-2 between the US + MB group and the other three groups (▲ $P < 0.01$ versus control group; ★ $P < 0.01$ versus MB group; $^{*}P < 0.01$ versus US group). There was a significant difference of VEGF between the US + MB group and the other three groups (★ $P < 0.01$ versus control group; ▲ $P < 0.01$ versus MB group;$^{*}P < 0.01$ versus US)

Discussion

Inertial cavitation is the main bioeffect underlying the therapeutic usefulness of low-frequency US, which has gained much attention in recent years.[31] The threshold for onset of cavitation depends on the presence of cavitation nuclei of appropriate size. In regards to *in vivo* blood circulation, bubbles have not been observed to occur naturally *in vivo* except in the digestive and respiratory tracts. Given the absence of cavitation nuclei in tumor blood circulation, cavitation at low acoustic pressures *in vivo* depends on the injection of stabilized bubbles. In this experiment, we found some bioeffects of rabbit hepatic tumors sonicated by low-frequency US and MBs injected through the auricular vein.

Apparent tumor coagulation necrosis, internal calcification, and diffuse hemorrhage were found in the US + MB group according to the H–E staining results. However, in the control, MB, and the US groups, there were no obvious changes in the tumor cells, and the vasculature in the tumors was intact. The mechanism of the observed results may play some role in blood vessels, as in the US + MB group, the MBs were injected into the tumor microcirculation. Periodic expansion, contraction, and eventual disruption of the MBs in the blood vessel focused by the external acoustic field have certain biological effects on adjacent vessel wall in the tumor tissue. Chen *et al.* used a high-speed photomicrography system to directly observe the dynamics of bubbles inside blood vessels in *ex vivo* rat mesenteries.[32] The behavior of MBs under irradiation with 1 MHz US has been studied in detail. Vascular bioeffects include vessel distention as the bubble expands irradiated by external US,[32,33] and then vessel invagination as the bubble collapses, producing a notch-like shape on both sides of the vessel wall suggesting high strains on the vessel wall. When bubble expansion is constrained by the vessel wall and surrounding tissue, the rebounding of the vessel wall during bubble collapse can 'inject' momentum back into the liquid[34,35] and lead to the formation of liquid jets.[36] Liquid jets arising from the collapse of MBs can locally produce transient holes.[37] The shear produced by the jets may affect the neighboring tissue structures and rupture vascular endothelial cell or blood vessel walls.[8] Although the behavior of MBs under irradiation with 20 kHz US has not been studied in detail in previous reports, but we infer that the sonication effect is more obvious at 20 kHz than that at 1 MHz as the cavitation effects are more obvious at the lower frequency used.[26] The lower the frequency of the wave is, the more time the bubble has to grow in the expansion half-cycle, and consequently, a more violent collapse during the following compression half-cycle results. Accordingly, it is reasonable to expect that the influence of transient cavitation will be more significant at lower ultrasonic frequencies.[20] In the future, available high-speed photomicrography systems may be used to study the relationship between the MB sonicated by 20 kHz US and the blood vessel *in vivo*. Using TEM, we found vascular endothelial cell ruptures, enlarged

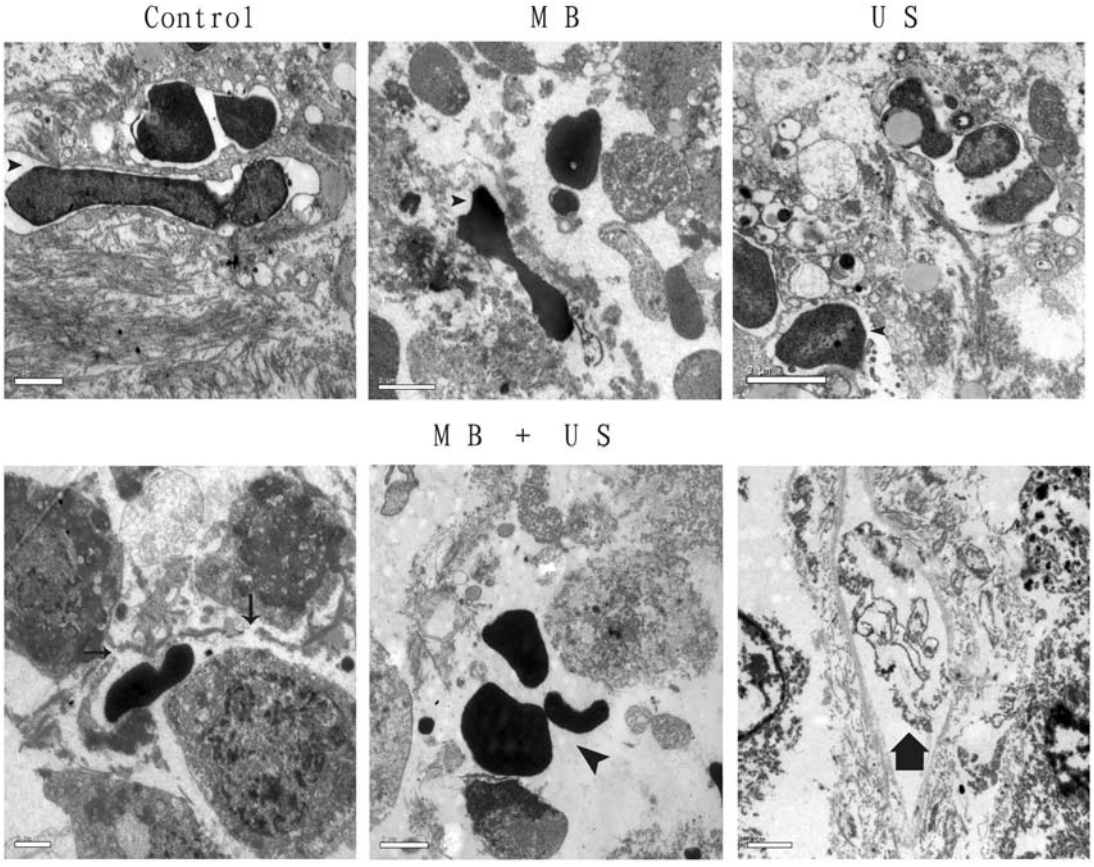

Figure 7 Microvessels of TEM in the control, MB, and US groups had an intact vascular lumen and normal erythrocytes in the vessels (arrow head); ruptured vascular endothelial cells, widened endothelial cell gap (slim arrow), erythrocyte exudation (arrow head), and microvascular thrombosis (course arrow) was observed in the US + MB group (scale: 2 μm).

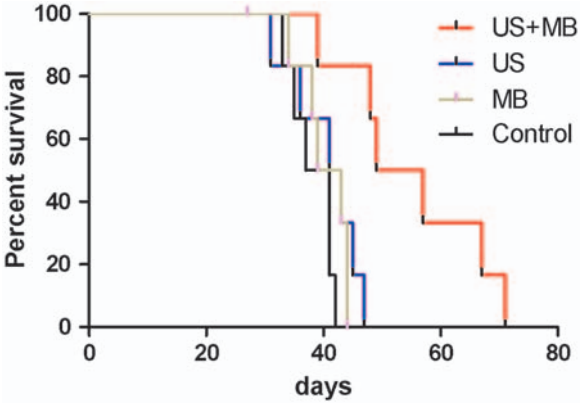

Figure 8 Rabbits treated with US + MB had a significantly longer overall survival than those in the control, MB, and US groups ($\chi 2 = 9.328$, $P = 0.0242$) (A color version of this figure is available in the online journal)

endothelial cell gaps, and red cell aggregation. It has been proposed that the US focused destruction of MBs increases the capillary permeability at the cellular microvascular level,[13] and the application of focused-US MB destruction can result in local hemorrhage.[38,39]

In our research, MBs exposed to low-frequency US caused the rupture of microvessels and interstitial extravasation of red cells or diffuse hemorrhage. Blood vessel deformations on microsecond time scales caused by ultrasonic cavitation,[32,40] including vessel distention, invagination, and liquid jets, can contribute to vessel rupture.[32,33] They may also cause a transient increase in temperature (reportedly up to 5000 K) that alters the fluidity of the cell membrane.[41,42] Local deposition of such high energy may result in the production of free radicals, which most likely cause cell damage that enhances the permeability of endothelial cell layers.[43] Passage of the erythrocytes into the intracellular space is facilitated through the widened endothelial cell gaps, at least in part as a result of acoustic cavitation of the membrane of vascular endothelial cells. These mechanisms may be used to explain why the enlarged endothelial cell gaps, endothelial cells rupture, and tissue hemorrhage were found in the US + MB group. We believe that long-term microvascular damage and ischemia eventually result in coagulation necrosis and calcification of rabbit hepatic tumors.

In our experiment, we found that the tumor volume of the US + MB group was significantly smaller than those in the three control groups. These results were similar to those of Liu et al.,[44] who researched the tumor vasculature of rats insonated percutaneously with an intravenous injection of a lipid MB. They found that the circulation of tumors could be completely blocked off for 24 h in treated tumors.

Histology revealed that the tumor microvasculature was disrupted into diffuse hematomas accompanied by intercellular edema, multiple cysts formation, and thrombosis. In our study, thrombosis is one of the phenomena of the tumor sonicated by US + MB. We hypothesize that when the vascular endothelial cells were damaged and degenerated by free radicals and liquid jets induced by US and MB, and erythrocytes and platelets perhaps stuck firmly on the surface of endothelial cells and exposed collagen fiber, resulting in increasing viscosity and resistance of blood flow, decreasing blood flow velocity, followed by further red blood cells, platelet adhesion to the wall, and eventual clot formation.

COX-2 and VEGF play critical roles in cancer angiogenesis.[45,46] Overexpression of COX-2 has been demonstrated to contribute to the carcinogenesis by stimulating cell proliferation, inhibiting apoptosis, and enhancing angiogenesis. In the present study, the results revealed that low-frequency US combined with MBs significantly downregulated the expression of COX-2 and VEGF, which was attributed to the promotion of apoptosis of cancer cells, leading to suppression of tumorigenesis. Other authors have also reported that when the microvessels are damaged, the expression of microvascular density (MVD) and VEGF is reduced, and angiogenesis is effectively inhibited.[47] The mechanism may be that blood vessel rupture and reduction of blood flow caused by endothelial cell injury, apoptosis, reduction, and loss which lead to the decreased expression of VEGF by the inhibition of PI3K/Akt pathway and ras-dependent signaling pathways.[48]

Hwang et al.[49] reported that in an *in vivo* rabbit auricular blood vessel model, acoustic cavitation nucleated with a MB contrast agent can damage the endothelia of veins at relatively low spatial-peak temporal-average intensities. That damage was proportional to the peak negative pressure amplitude of the insonifying pulses. US contrast agent-induced endothelial damage can be inherently thrombogenic. In our research, we exerted longer treatment of approximately 2 weeks, and apparent hepatic tumor growth inhibition was found. In the US + MB group, diffused thrombi were observed in the microvasculature, and the survival time of rabbits was longer than those in the control, MB, and US groups. Angiogenesis is of vital importance to the growth and metastasis of solid tumors. Vessel damage, such as endothelial cells rupture, enlarged cell gaps, and thrombogenesis, may be the fundamental reasons why the tumor growth in the US + MB group was inhibited and rabbits in the US + MB group had a longer survival time.

There were some limitations to our study. First, although US in combination with MB had an effect on the vessel that was related to protein expression in the tumor tissue, US alone had a few effects on the tumor tissue. Thus, the exact mechanism of vascular damage has not been fully elucidated in our study and requires further research. Second, the potential adverse effects on blood vessels in normal tissues were not investigated in the US + MB group and thus require further exploration in the future.

In conclusion, erythrocytes can pass into the intracellular compartment via the process of cavitation when facilitated with focused US. Appropriate energy US to cellular damage is a desirable effect of focused low-frequency US. Low-frequency US combined with MBs slowed tumor growth, reduced VEGF and COX-2 expression, along with vascular endothelial cell wall rupture, red blood cell leakage, and promoted longer rabbit survival. The results may lay the foundation for the future clinical application of low-frequency US and MBs.

As noted earlier, there is considerable uncertainty to date regarding the mechanisms underlying the well documented but poorly understood observations of enhanced *in vivo* microvasculature damage in the presence of MBs exposed to low-frequency US. More subtle effects on the scale of the vascular endothelial cells may be involved than was previously thought. This phenomenon has only recently begun to be investigated in detail, and future developments will be of great importance in optimizing the use of MBs in therapeutic procedures.

Author contributions: Guarantors of integrity of entire study: Z-Y S, BH; study concepts, BH, ES; study design, Z-Y S, BH, G-L X, M-F W; literature research, ES, M-X S, F-L Q; data acquisition, Z-Y S, G-L X, M-F W, M-X S; data analysis/interpretation, Z-Y S, G-L X, M-F W; statistical analysis, M-X S, F-L Q; manuscript preparation, Z-Y S, G-L X; manuscript definition of intellectual content, Z-Y S, BH; manuscript editing, Z-Y S, BH; and manuscript revision/review and final version approval, all authors.

ACKNOWLEDGMENTS

This work was supported in part by The National Natural Science Foundation of China (81271597). We thank general managers Xin Yue Gan and Xun Shen for their provision of the ultrasound therapy apparatus. Shu liang Nan and Yan Duan Lin kindly provided us with tumor cell line. Jun Yan Yang and Jia Jin Liu provided us with ultrasound contrast agent. We thank Hai Feng Shi and Chun Yan Han for helping with the tumor inoculation. We also thank Yu Qing Zhou, Yu Feng Chen, Jun Lian Yuan, Lu Hua Yang, Lei Yan Ji, and Ai Yan Fu for their help with the imaging examination of rabbits.

REFERENCES

1. Alzaraa A, Gravante G, Chung WY, Al-Leswas D, Bruno M, Dennison AR, Lloyd DM. Targeted microbubbles in the experimental and clinical setting. *Am J Surg* 2012;**204**:355–66
2. Yeh CK. Ultrasound microbubble contrast agents for diagnostic and therapeutic applications: Current status and future design. *Chang Gung Med J* 2012;**35**:125–39
3. Guang Y, Xie LM, Ding H, Cai AL, Huang Y. Diagnosis value of focal liver lesions with SonoVue®-enhanced ultrasound compared with contrast-enhanced computed tomography and contrast-enhanced MRI: A meta-analysis. *J Cancer Res Clin Oncol* 2011;**137**:1595–605
4. Klibanov AL. Microbubble contrast agents: Targeted ultrasound imaging and ultrasound-assisted drug-delivery applications. *Invest Radiol* 2006;**41**:354–62
5. Frenkel V. Ultrasound mediated delivery of drugs and genes to solid tumors. *Adv Drug Deliv Rev* 2008;**60**:1193–208
6. Escoffre J-M, Zeghimi A, Novell A, Bouakaz A. In-vivo gene delivery by sonoporation: Recent progress and prospects. *Curr Gene Ther* 2013;**13**:2–14

7. Doinikov AA, Bouakaz A. Acoustic microstreaming around an encapsulated particle. *J Acoust Soc Am* 2010;**127**:1218–27
8. Pereira AH, Tirapelli C, Rodolpho LA. Ultrasonic dental scaler performance assessment with an innovative cavitometer. *Am J Appl Sci* 2010;**7**:290–300
9. Zhou Y, Cui J, Deng CX. Dynamics of sonoporation correlated with acoustic cavitation activities. *Biophys J* 2008;**94**:L51–3
10. Ohl C-D, Wolfrum B. Detachment and sonoporation of adherent HeLa-cells by shock wave-induced cavitation. *Biochim Biophys Acta* 2003;**1624**:131–8
11. Ohl C-D, Arora M, Ikink R, de Jong N, Versluis M, Delius M, Lohse D. Sonoporation from jetting cavitation bubbles. *Biophys J* 2006;**91**:4285–95
12. Yuan F, Sankin G, Zhong P. Dynamics of tandem bubble interaction in a microfluidic channel. *J Acoust Soc Am* 2011;**130**:3339–46
13. Stride E, Coussios C. Cavitation and contrast: The use of bubbles in ultrasound imaging and therapy. *Proc IMechE, Part H: J Engineering in Medicine* 2010;**224**:171–91
14. Jamaluddin A, Ball G, Turangan C, Leighton T. The collapse of single bubbles and approximation of the far-field acoustic emissions for cavitation induced by shock wave lithotripsy. *J Fluid Mech* 2011;**677**:305–41
15. Cool SK, Geers B, Lentacker I, De Smedt SC, Sanders NN. Enhancing nucleic acid delivery with ultrasound and microbubbles. *Methods Mol Biol* 2013;**948**:195–204
16. Escoffre J-M, Novell A, Serrière S, Lecomte T, Bouakaz A. Irinotecan delivery by microbubble-assisted ultrasound: In-vitro validation and a pilot preclinical study. *Mol Pharm* 2013;**10**:2667–75.
17. Wang S, Shin IS, Hancock H, Jang B-S, Kim H-S, Lee SM, Zderic V, Frenkel V, Pastan I, Paik CH. Pulsed high intensity focused ultrasound increases penetration and therapeutic efficacy of monoclonal antibodies in murine xenograft tumors. *J Control Release* 2012;**162**:218–24
18. Krasovitski B, Frenkel V, Shoham S, Kimmel E. Intramembrane cavitation as a unifying mechanism for ultrasound-induced bioeffects. *Proc Natl Acad Sci USA* 2011;**108**:3258–63
19. Delalande A, Postema M, Mignet N, Midoux P, Pichon C. Ultrasound and microbubble-assisted gene delivery: Recent advances and ongoing challenges. *Ther Deliv* 2012;**3**:1199–215
20. Ahmadi F, McLoughlin IV, Chauhan S, ter-Haar G. Bio-effects and safety of low-intensity, low-frequency ultrasonic exposure. *Prog Biophys Mol Biol* 2012;**108**:119–38
21. Mitragotri S. Healing sound: The use of ultrasound in drug delivery and other therapeutic applications. *Nat Rev Drug Discov* 2005;**4**:255–60
22. Shen ZY, Shen E, Zhang JZ, Bai WK, Wang Y, Yang SL, Nan SL, Lin YD, Li Y, Hu B. Effects of low-frequency ultrasound and microbubbles on angiogenesis-associated proteins in subcutaneous tumors of nude mice. *Oncol Rep* 2013;**30**:842–50
23. Todorova M, Agache V, Mortazavi O, Chen B, Karshafian R, Hynynen K, Man S, Kerbel RS, Goertz DE. Antitumor effects of combining metronomic chemotherapy with the antivascular action of ultrasound stimulated microbubbles. *Int J Cancer* 2013;**132**:2956–66
24. Zhou SJ, Li SW, Wang JJ, Liu ZJ, Yin GB, Gong JP, Liu CA. High-intensity focused ultrasound combined with herpes simplex virus thymidine kinase gene-loaded ultrasound-targeted microbubbles improved survival of rabbit with VX2 liver tumor. *J Gene Med* 2012;**14**:570–9
25. Wu F, Wang Z-B, Chen W-Z, Zou J-Z, Bai J, Zhu H, Li K-Q, Jin C-B, Xie F-L, Su H-B. Advanced hepatocellular carcinoma: Treatment with high-intensity focused ultrasound ablation combined with transcatheter arterial embolization. *Radiology* 2005;**235**:659–67
26. Ueda H, Mutoh M, Seki T, Kobayashi D, Morimoto Y. Acoustic cavitation as an enhancing mechanism of low-frequency sonophoresis for transdermal drug delivery. *Biol Pharm Bull* 2009;**32**:916–20
27. Greis C. Technology overview: SonoVue (Bracco, Milan). *Eur Radiol* 2004;**14**:11–15
28. Yu SM, Kim SJ. Endoplasmic reticulum stress (ER-stress) by 2-deoxy-D-glucose (2DG) reduces cyclooxygenase-2 (COX-2) expression and N-glycosylation and induces a loss of COX-2 activity via a Src kinase-dependent pathway in rabbit articular chondrocytes. *Exp Mol Med* 2010;**42**:777–86
29. Forsberg F, Dicker AP, Thakur ML, Rawool NM, Liu J, Shi WT, Nazarian LN. Comparing contrast-enhanced ultrasound to immunohistochemical markers of angiogenesis in a human melanoma xenograft model: Preliminary results. *Ultrasound Med Biol* 2002;**28**:445–51
30. Kahn E, Tissot N, Frere P, Dauphin A, Boumhras M, Bachelet C-M., Frouin F, Lizard G. Fluorescence excitation analysis by two-photon confocal laser scanning microscopy: A new method to identify fluorescent nanoparticles on histological tissue sections. *Int J Nanomed* 2012;**7**:5545–54
31. Feril LB Jr, Kondo T. Biological effects of low intensity ultrasound: The mechanism involved, and its implications on therapy and on biosafety of ultrasound. *J Radiat Res* 2004;**45**:479–89
32. Chen H, Brayman AA, Bailey MR, Matula TJ. Blood vessel rupture by cavitation. *Urol Res* 2010;**38**:321–26
33. Chen H, Brayman AA, Bailey MR, Matula TJ. Direct observation of microbubble interactions with ex vivo microvessels. *J Acoust Soc Am* 2009;**125**:2680
34. Leppinen D, Wang Q, Blake J. Pulsating bubbles near boundaries. *Bubble Dyn Shock Waves* 2012;**8**:33–65
35. Brujan EA, Matsumoto Y. Collapse of micrometer-sized cavitation bubbles near a rigid boundary. *Microfluidics Nanofluidics* 2012;**13**:957–66
36. Pain A, Hui Terence Goh B, Klaseboer E, Ohl SW, Cheong Khoo B. Jets in quiescent bubbles caused by a nearby oscillating bubble. *J Appl Phys* 2012;**111**:054912–9
37. Cravotto G, Gaudino EC, Cintas P. On the mechanochemical activation by ultrasound. *Chem Soc Rev* 2013;**42**:7521–34
38. Gao Y, Gao S, Zhao B, Zhao Y, Hua X, Tan K, Liu Z. Vascular effects of microbubble-enhanced, pulsed, focused ultrasound on liver blood perfusion. *Ultrasound Med Biol* 2012;**38**:91–8
39. Tinkov S, Bekeredjian R, Winter G, Coester C. Microbubbles as ultrasound triggered drug carriers. *J Pharm Sci* 2009;**98**:1935–61
40. Chen H, Kreider W, Brayman AA, Bailey MR, Matula TJ. Blood vessel deformations on microsecond time scales by ultrasonic cavitation. *Phys Rev Lett* 2011;**106**:34301
41. Suslick KS, Flannigan DJ. Inside a collapsing bubble: sonoluminescence and the conditions during cavitation. *Annu Rev Phys Chem* 2008;**59**:659–83
42. Holland CK, Apfel RE. An improved theory for the prediction of microcavitation thresholds. *IEEE Trans Ultrason Ferroelectr Freq Control* 1989;**36**:204–8
43. Basta G, Venneri L, Lazzerini G, Pasanisi E, Pianelli M, Vesentini N, Del Turco S, Kusmic C, Picano E. In vitro modulation of intracellular oxidative stress of endothelial cells by diagnostic cardiac ultrasound. *Cardiovasc Res* 2003;**58**:156–61
44. Liu Z, Gao S, Zhao Y, Li P, Liu J, Tan K, Xie F. Disruption of tumor neovasculature by microbubble enhanced ultrasound: A potential new physical therapy of anti-angiogenesis. *Ultrasound Med Biol* 2011;**38**:253–61
45. Şahin M, Şahin E, Gümüşlü S. Cyclooxygenase-2 in cancer and angiogenesis. *Angiology* 2009;**60**:242–53
46. Zhang J, Ye J, Ma D, Liu N, Wu H, Yu S, Sun X, Tse W, Ji C. Cross-talk between leukemic and endothelial cells promotes angiogenesis by VEGF activation of the Notch/Dll4 pathway. *Carcinogenesis* 2013;**34**:667–77
47. Chen L, Li N, Ye H. The effect of high intensity focused ultrasound on vascular endothelial growth factor and microvessel density in rabbit V-X2 hepatocellular carcinoma models. *Hepatogastroenterology* 2013;**60**:136–9
48. Dimmeler S, Zeiher AM. Endothelial cell apoptosis in angiogenesis and vessel regression. *Circ Res* 2000;**87**:434–9
49. Hwang JH, Brayman AA, Reidy MA, Matula TJ, Kimmey MB, Crum LA. Vascular effects induced by combined 1-MHz ultrasound and microbubble contrast agent treatments in vivo. *Ultrasound Med Biol* 2005;**31**:553–64

(Received October 11, 2013, Accepted January 15, 2014)